J Physiol Sci (2018) 68:345–353
https://doi.org/10.1007/s12576-017-0537-9

ORIGINAL PAPER

A rotating cerium anode X-ray system allows visualization of intramural coronary vessels after cardiac stem cell therapy for myocardial infarction

Chiharu Tanaka[1] · Toru Hosoda[2] · Yoshimori Ikeya[3] · Yoshiro Shinozaki[4] · Kikue Todoroki[3] · Toru Shizuma[3] · Takashi Shiraishi[5] · Naoto Fukuyama[3] · Toshihiko Ueda[1] · Hidezo Mori[3]

Received: 18 January 2017 / Accepted: 5 April 2017 / Published online: 12 April 2017

Abstract Conventional angiography is insufficient for evaluating the therapeutic effect of cardiac regeneration therapy. A microangiographic X-ray system using a cerium anode was developed. Cerium has a characteristic X-ray with a peak at 34.6 keV, which allows visualization of tiny amounts of iodine. The performance of the cerium anode X-ray system was evaluated in two excised normal canine hearts and in excised ischemic canine hearts treated with c-kit-positive cardiac stem cells (5 canines) or without cells (5 control canines). In the normal canines, branches penetrating from the left anterior descending artery into the myocardium were visualized, down to third-order branches. In just the treated hearts treated with stem cells, small vessels characterized by irregular vessel walls were observed. The cerium anode X-ray system allowed visualization of microvessels in excised ischemic canine hearts, and may evaluate the effect of cardiac stem cell therapy.

✉ Chiharu Tanaka
chitty@is.icc.u-tokai.ac.jp

✉ Hidezo Mori
coronary@is.icc.u-tokai.ac.jp

[1] Department of Cardiovascular Surgery, Tokai University School of Medicine, 143 Shimokasuya, Isehara, Kanagawa 259-1193, Japan

[2] Tokai University Institute of Innovative Science and Technology, 143 Shimokasuya, Isehara, Kanagawa 259-1193, Japan

[3] Department of Physiology, Tokai University School of Medicine, 143 Shimokasuya, Isehara, Kanagawa 259-1193, Japan

[4] Support Center for Medical Research and Education, Tokai University School of Medicine, 143 Shimokasuya, Isehara, Kanagawa 259-1193, Japan

[5] NHK Engineering Services, Inc., Tokyo, Japan

Keywords Microangiography · C-kit-positive cardiac stem cells · Cerium anode · Myocardial infarction · Canine models

Background

Regenerative therapy using stem cells has substantial potential to save patients from severe heart failure, and may thus decrease medical costs [1–3]. The two major goals of cardiac stem cell therapy are the regeneration of myocardial tissue and the reconstruction of the coronary vascular system. However, in clinical settings, tools to evaluate the effects of stem cell therapy on the coronary system are insufficient [4, 5]. Although coronary angiography is considered the best method for assessing the coronary arterial system, the spatial resolution of clinically available angiography is limited ($\geq$100–200 μm). A new angiographic device with a higher resolution is needed to examine the efficacy of regenerative therapy on the heart in clinical settings.

Cardiac stem cells in the adult heart which express the stem cell antigen, c-kit, contribute to cardiomyocyte regeneration and vascular turnover [6, 7]. C-kit-positive cardiac stem cells (CSCs) are stored in cardiac niches, migrate to the damaged tissue, and replace the native cells [7]. A heart with scar tissue after a myocardial infarction has little capacity to generate new cardiomyocytes [8]. Human c-kit-positive CSCs can substitute viable cardiomyocytes and vascular structures over dead tissue in infarcted hearts of immunocompromised animals [9, 10]. Additionally, according to the report on the SCIPIO trial, the left ventricular ejection fraction increased and the infarct size decreased after infusion of c-kit-positive CSCs in patients who underwent coronary artery bypass grafting

after myocardial infarction [11, 12], and the adverse effects of this intervention have not been reported thus far [7].

We developed a new microangiographic system using a rotating cerium anode, confirmed the ability of the system in detection of small coronary vessels and their diameter quantification, and applied the system to assess the effects of CSC injection on the ischemic myocardium following coronary ligation.

Methods

Microangiographic X-ray system using a rotating cerium anode

We successfully developed a microangiographic X-ray system using a cerium anode (Fig. 1). Iodine contrast materials are widely used in clinical settings. The peak mass attenuation coefficient of iodine is at 33.2 keV, which is termed as the K-edge of iodine. The differences in the mass attenuation coefficient between the human body and iodine contrast materials produces the angiographic contrast, which becomes maximum around the K-edge of iodine [13–16]. Therefore, the new system with a cerium anode has advantages in detecting tiny amounts of iodine in small vessels. The cerium anode X-ray system is characterized by an X-ray spectrum with a peak intensity at 34.6 keV (just above the K-edge of iodine) and a relatively narrow distribution with a half-maximum width of 10 keV.

The detector for this X-ray system is a highly sensitive, high-definition flat panel (Hamamatsu Photonics, Shizuoka, Japan) coupled with image acquisition software, HiPic 7.0 (Hamamatsu Photonics), which had a spatial resolution of 50 μm.

Adobe photoshop CC 2015.5 was used to create the artworks.

Animal experiments

The investigation confirms with The Guide for the Care and Use of Laboratory Animals published by the US. National Institutes of Health (NIH Publication No. 85-23, revised 1996). All procedures performed in studies involving animals were in accordance with the ethical standards of Tokai University School of Medicine (Kanagawa, Japan) at which the studies were conducted.

Microangiography of excised hearts from normal canines

Two canines were employed for these experiments (female beagles, 27 months of age, weighing 9.9 kg in all, and bred at Kichijo Farm, Gifu, Japan). Each canine was anesthetized with an intravenous injection of midazolam (0.4 mg/kg), dexmedetomidine (20 μg/kg), and butorphanol (0.3 mg/kg) as a bolus infusion, then given propofol 6 mg/kg/h for maintenance during the operation, and intubated thereafter. Each canine was kept in the right lateral position. The heart was exposed following a left thoracotomy at the fifth intercostal space. A small catheter was inserted into the proximal site of the left anterior descending (LAD) artery. Thereafter, $3–5 \times 10^8$ iodine microspheres, with a diameter of 15 μm and 37% iodine by weight, were injected to fill the coronary arterial system [17, 18]. Injection was continued until the coronary branches were filled up with the microspheres and turned white. The proximal LAD artery was ligated. The heart was then excised, fixed in formalin for a few weeks, and imaged by microangiography using the cerium anode X-ray system as well as by conventional angiography. The visualized microvessels were statistically analyzed.

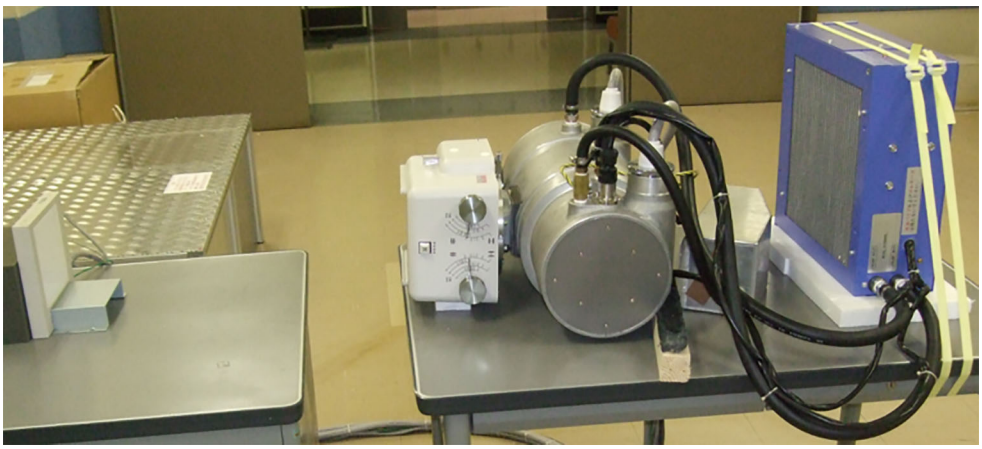

Fig. 1 A new microangiographic X-ray system using a cerium anode. The cerium anode X-ray system is sufficiently small to be utilized in hospitals

Microangiography of the c-kit-positive CSC model

Ten canines were used for this experimental protocol (female beagles, 11–13 months of age, weighing 9.8–10.8 kg, and obtained from Kitayama Labs, Yamaguchi, Japan). Five were treated with autologous c-kit-positive CSCs (CSC group), and five were treated with saline (control group). Each canine was anesthetized and given maintenance anesthesia during the operation as described above. The left atrium was exposed following a left thoracotomy at the third intercostal space, and the left atrial appendage was excised, sutured continuously using 4-0 nylon, and the chest was closed. Each canine was intensively cared for after the surgery. The extracted cardiac tissue was pulverized. After dissociating with 2 mg/ml collagenase (NB4; Serva, Heidelberg, Germany), cardiac cells were seeded on dishes, and colonies were cultured in Ham's F12 Nutrient Mixture (HyClone SH30026; Thermo Scientific, MA, USA) supplemented with 10% fetal bovine serum (HyClone SH30406.02; Thermo Scientific), 10 ng/ml basic fibroblast growth factor (100.18B; Peprotech, NJ, USA), 5 units/L erythropoietin (E5627; Sigma-Aldrich, MI, USA), 0.2 mM glutathione (G6013; Sigma-Aldrich), and antibiotics. The culture medium was changed every 2–3 days. C-kit-positive CSCs were selected using the MACS Micro Bead Technology with human CD117 microbeads (130-091-332; Miltenyi Biotec, Bergisch Gladbach, Germany). Some CSCs were stained with the anti-c-kit antibody and 4′,6-diamidino-2-phenylindole (DAPI).

A second surgery was performed 1 month later. Each canine was anesthetized, and left ventriculography (LVG) was performed to ascertain the presence of intact cardiac contraction without asynergy. After a left thoracotomy at the fifth intercostal space was performed, we pretreated canines with 2 mg/kg lidocaine and 1000 IU heparin intravenously for preventing arrhythmia and thrombus. The LAD artery and its collateral branches were ligated to create a severe ischemic area in the apical region of each heart. Echocardiograms were obtained just before and after the coronary ligation to confirm the wall motion abnormality induced by the procedure. Subsequently, in the 5 canines in the CSC group, 1×10^6 of c-kit-positive CSCs in 5 ml of glucose-lactated Ringer's solution (Physio 140 injection; Otsuka Pharmaceutical Factory, Tokyo, Japan) were injected via multiple injections directly to the ischemic myocardium along the borderline of the non-ischemic zone. Following LVG, the chest was closed. The canines were carefully managed for 1 month prior to a third operation. After anesthesia and LVG, each heart was excised. The coronary artery was catheterized from the ascending aorta and filled with concentrated barium [19]. Thereafter, the excised heart was irradiated to assess microvessels. The 5 control canines were examined in the same manner, but 5 ml of glucose-lactated Ringer's solution was administered to each heart instead of CSCs.

Angiography using the cerium anode X-ray system and the conventional system

The hearts were irradiated using the cerium anode X-ray system. The energy was adjusted by changing the voltage, the electric current, and the exposure time, which ranged from 60 to 100 kV, from 50 to 100 mA, and from 100 to 20,000 ms, respectively. A 10- or 20-cm-thick acrylic plate was placed between the X-ray tube and the heart to simulate the thickness of a human body. The visualized vessels were compared to a guide wire of 100 μm in diameter to quantitate the dimensions of microvessels.

To compare image qualities between the two X-ray systems, the irradiation by conventional X-ray system was performed using Radiotex Safire R-30H (Shimadzu, Kyoto, Japan), which has an X-ray tube voltage of 40–150 kV.

In a normal dog, we compared numbers of visualized epicardial coronary arteries (EPCA) and their branches, penetrating intramural coronary arteries (IMCA) and their branches between the cerium anode X-ray system and the conventional X-ray system. We also quantitated the vessels' diameter reduction at the branching junction and compared their reduction rate at EPCAs and their branches, and at IMCAs and their branches.

Results

Microangiography of the excised hearts from normal canines

As shown in Figs. 2 and 3, in normal canines, IMCA penetrating from the LAD artery into the myocardium were visualized by both the cerium anode X-ray system and the conventional angiographic system set at 100 kV, 50 mA, and 100 ms of tube voltage, current, and exposure time, respectively. Second-order branches were visualized by both systems as indicated by the white delta symbols in Figs. 2b and 3b. The third-order branches could be visualized in some daughter branches of 2nd-order branches of IMCAs; 50% (14/28) by the cerium anode X-ray system and 33% (6/20) by the conventional X-ray system (Table 1). In order to simulate X-ray absorption of skin, muscles, and bones of an adult human, we placed a 20-cm-thick acrylic plate between the X-ray tube and the excised heart. The images of IMCA in the both X-ray systems became blurred (indicated by the white delta symbols in Figs. 4 and 5) by the acrylic plate placement with the settings of 100 kV, 50 mA, and 1000 ms of tube voltage,

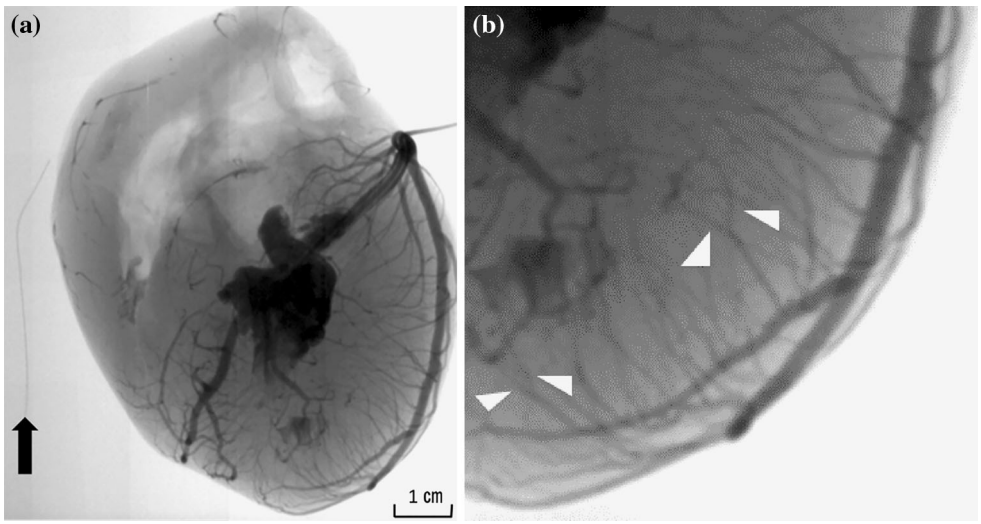

Fig. 2 An excised heart irradiated by the cerium anode X-ray system. **a** The image was obtained by the cerium anode X-ray system set at 100 kV, 50 mA, and 100 ms of tube voltage, current, and exposure time, respectively. A guide wire with a diameter of 100 μm (*black arrow* in Fig. 3a) is used for calibration to measure the vessel diameters. **b** This is a magnified image of (**a**). It shows many IMCAs from EPCA down to the third-order branches as indicated by the *white delta symbol*

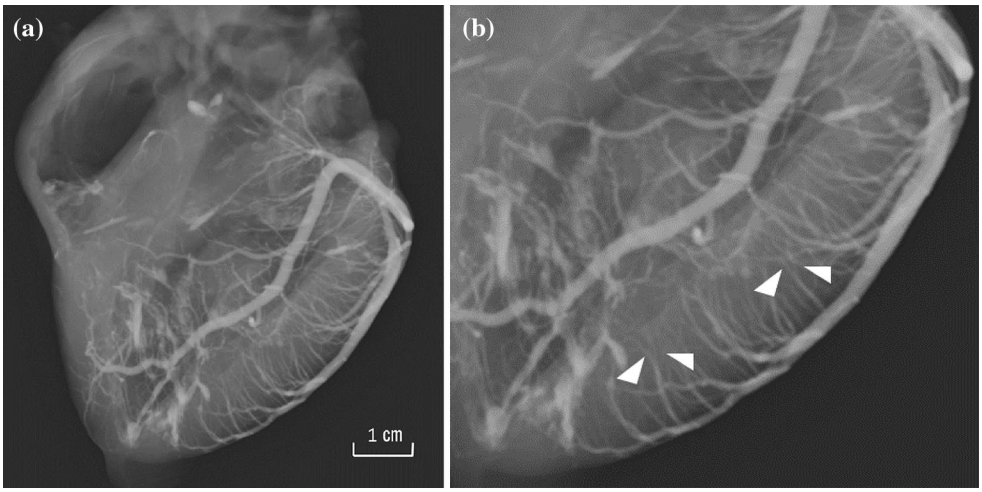

Fig. 3 An excised heart irradiated by the conventional X-ray system. **a** The image was obtained by the conventional X-ray system set at 100 kV, 50 mA, and 100 ms of tube voltage, current, and exposure time, respectively. **b** This is a magnified image of (**a**). The IMCA second-order branches were visualized as indicated by the *white delta symbol*

current, and exposure time, respectively. However, the image quality of IMCA was better maintained with the cerium anode X-ray system than the conventional system (tube voltage, current, and exposure time were set equally) (Fig. 4). As summarized in Table 1, we compared the numbers of visualized EPCA and IMCA between the cerium anode and the conventional X-ray system. The cerium anode X-ray system visualized 44 of first-order branches, 28 of second-order branches, and 14 of third-order branches of IMCA. The placement of a 20-cm-thick acrylic plate decreased the number of visualized branches of IMCA, 70% (31/44) of first-order branches, 71% (20/28) of second-order branches, and 43% (6/14) of third-order branches compared with the condition without acrylic plate. On the other hand, the conventional X-ray system could visualize only 44% (18/41) of first-order branches, 25% (6/24) of second-order branches and 0% (0/4) of third-order branches of IMCA compared with the condition without acrylic plate. Mean diameters of the visualized vessels are also summarized in Table 1. In the condition without the acrylic plate, the cerium anode X-ray system demonstrated a drastic reduction of mean vessel diameter from 319.5 to 83.1 μm (reduction of 72.7%) at the branching from EPCA to first-order branches of IMCA, an ordinary reduction from 78.6 to 55.2 μm (reduction of 27.7%) at the branching junction of first- and second-order branches of IMCA, and from 75.0 to 52.4 μm (reduction of 30.9%) at the branching of the second- and third-order branches of IMCA.

Microangiography of the c-kit-positive CSC model

C-kit-positive CSCs were successfully cultivated to yield more than 1,000,000 cells for each canine ($n = 10$). CSCs

Table 1 Vessel diameter, number, and the reduction ratio at the junction of branching of EPCA and IMCA

Site of branching	No acrylic plate			With a 20-cm-thick acrylic plate		
	Number of branching	Measured diameter (μm)	Diameter reduction ratio[a] (%)	Number of branching	Measured diameter (μm)	Diameter reduction ratio[a](%)
The cerium anode X-ray system						
EPCA–IMCA first-order Br J	44	319.5 ± 86.7 to 83.1 ± 27.7	72.7	31	212.5 ± 60.2–51.2 ± 16.1	74.7
IMCA first–second-order Br J	28	78.6 ± 21.4 to 55.2 ± 12.8	27.7	20	52.0 ± 8.0–39.8 ± 5.6	22.8
IMCA second–third-order Br J	14	75.0 ± 16.1 to 52.4 ± 16.1	30.9	6	61.9 ± 13.3–38.1 ± 8.7	38.0
The conventional X-ray system						
EPCA–IMCA first-order Br J	41	375.5 ± 130.2 to 96.4 ± 15.0	70.9	18	436.4 ± 108.6–108.6 ± 26.3	70.5
IMCA first–second order Br J	24	91.2 ± 19.4 to 72.5 ± 15.1	19.1	6	139.3 ± 20.6–92.0 ± 24.3	33.4
IMCA second–third order Br J	4	78.6 ± 10.1 to 50.0 ± 0.0	35.8	0	92.0 ± 24.3/no data	–

Br J branching juncton

[a] (mother V. – daughter V./mother V.) × 100%

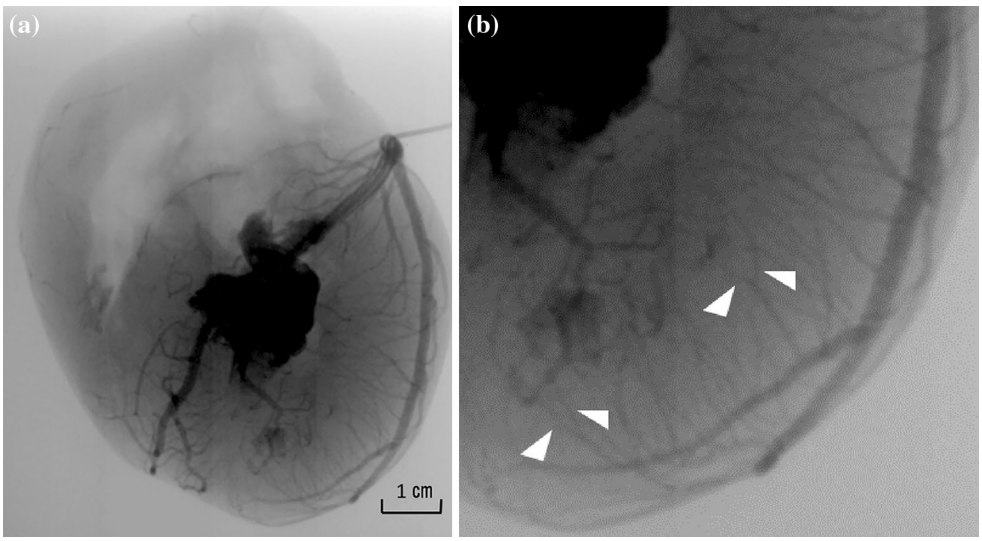

Fig. 4 An excised heart irradiated by the cerium anode X-ray system with a 20-cm-thick acrylic plate. **a** The image was obtained by the rotating cerium anode X-ray system set at 100 kV, 50 mA, and 1000 ms of tube voltage, current, and exposure time, respectively, after placing a 20-cm-thick acrylic plate between the X-ray tube and the excised heart. **b** This is a magnified image of (**a**). The third-order branches were sufficiently visualized as indicated by the *white arrow*

stained with the anti-c-kit antibody (red) and DAPI (blue) are shown in Fig. 6.

Ischemic changes were confirmed by electrocardiography to detect a depressed ST segment, and wall motion abnormality was detected by LVG before and after the coronary arterial ligation during the second surgery. Wall motion tended to decrease postoperatively compared to the preoperative examination and remained decreased for

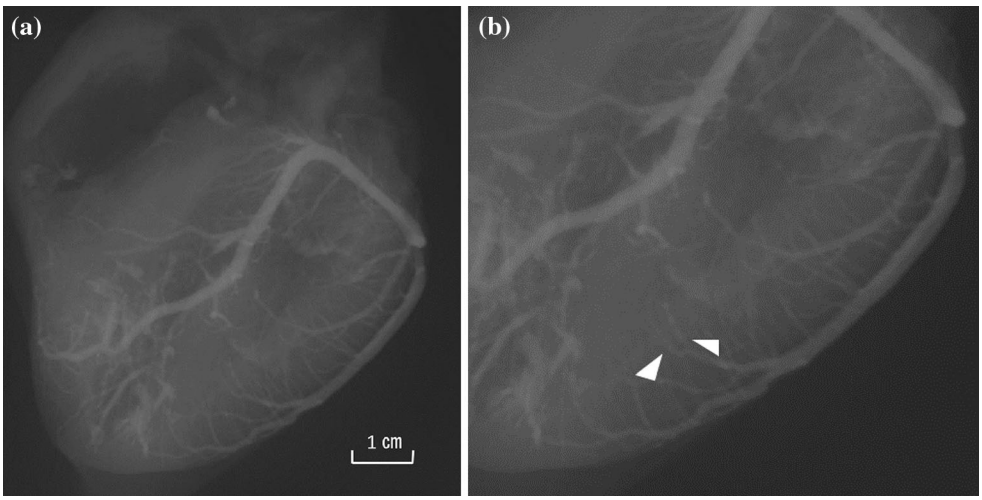

Fig. 5 An excised heart irradiated by the conventional X-ray system with a 20-cm-thick acrylic plate. **a** The image was obtained by the conventional X-ray system set at 100 kV, 50 mA, and 1000 ms of tube voltage, current, and exposure time, respectively, after placing a 20-cm-thick acrylic plate between the X-ray tube and the excised heart. **b** This is a magnified image of (**a**). The IMCA third-order branches from EPCA were poorly visualized as indicated by the *white arrow*

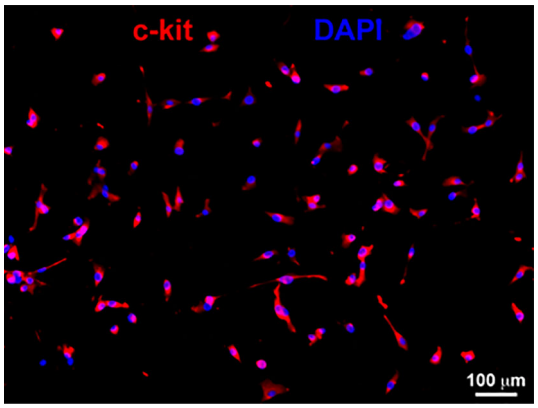

Fig. 6 Cardiac stem cells (CSCs) stained with the anti-c-kit antibody. c-kit-positive CSCs were stained in *red*. The nuclei were stained in *blue* with 4′,6-diamidino-2-phenylindole

1 month after the surgery. Two canines in the CSC group and three canines in the control group died due to lethal perioperative arrhythmia caused by the coronary ligation. All coronary microangiographic images of excised hearts were obtained 1 week after the third surgery for both groups, set at 100 kV, 80 mA, and 100 ms of tube voltage, current, and exposure time, respectively.

As shown in Fig. 7, in the to remaining control canines not treated with CSCs, an avascular area was noted at the apical heart region as indicated by the black delta symbol. Ligated LAD branches were visualized along the border zone of the ischemic area as indicated by the white delta symbol in Fig. 7b. Similar observations were recognized in all cases of the control group ($n = 2$). In contrast, in the CSC group (shown in Fig. 8, $n = 3$), multiple small vessels were clearly visualized in the apex as indicated by the white delta symbol in Fig. 8b. They were characterized by irregularities of the vessel wall and a coil-like shape. The irregular vessels were found in all cases of the CSC group.

Discussion

We successfully developed a cerium anode X-ray system (Fig. 1), confirmed better ability to detect small coronary vessels and their limitation of vascular diameter quantification (Figs. 2, 3, 4, 5; Table 1), and assessed its usefulness to evaluate the therapeutic effects of CSC treatment.

Theoretical background for newly developed cerium anode X-ray system

The newly developed X-ray system with a cerium anode has a K-edge at 33.2 keV, and, therefore, it has a better ability to detect small vessels than conventional X-ray systems. The X-ray spectrum of conventional X-ray systems using tungsten anodes range from 10 to 100 keV, and the peak intensity is much higher (69.5 keV) than the K-edge of iodine. Thus, the cerium anode X-ray system has a clear advantage over conventional X-ray systems for detecting iodine contrast materials in microvessels [20]. One disadvantage of the cerium anode X-ray system is that cerium is not heat-resistan, and it has a relatively low melting temperature. Tungsten, with a high melting point at 3683 K and a large heat capacity, is commonly used as an anode in angiographic systems. We applied a new system with a continuously rotating cerium anode to radiate heat.

Additionally, barium was used as the contrast material in the present study. Barium is also usable as contrast

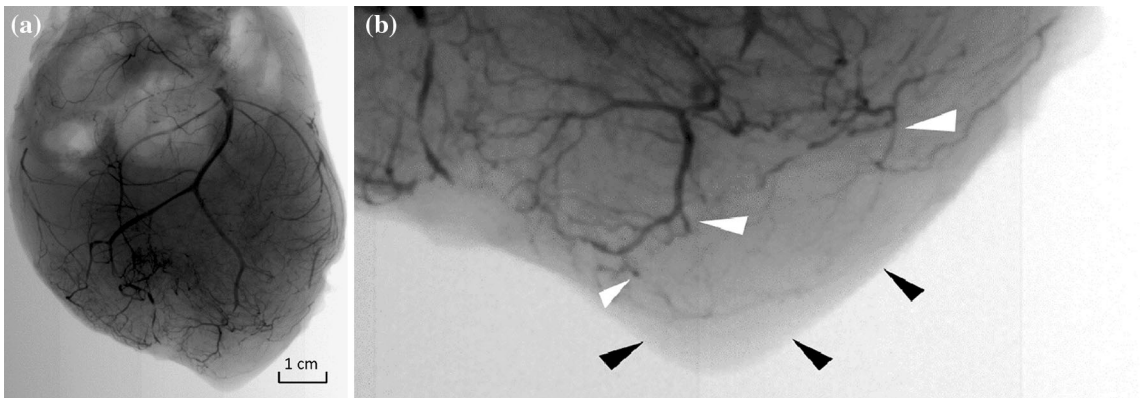

Fig. 7 An excised heart of a canine not treated with CSCs (control group). **a** The excised canine heart of the control group was exposed by the cerium anode X-ray system. **b** This is a magnified image of (**a**). An avascular bed at the heart apex (indicated by *black arrows*) and interrupted arteries in the border zone of the ischemic area (indicated by *white arrows*) were visualized in the control group

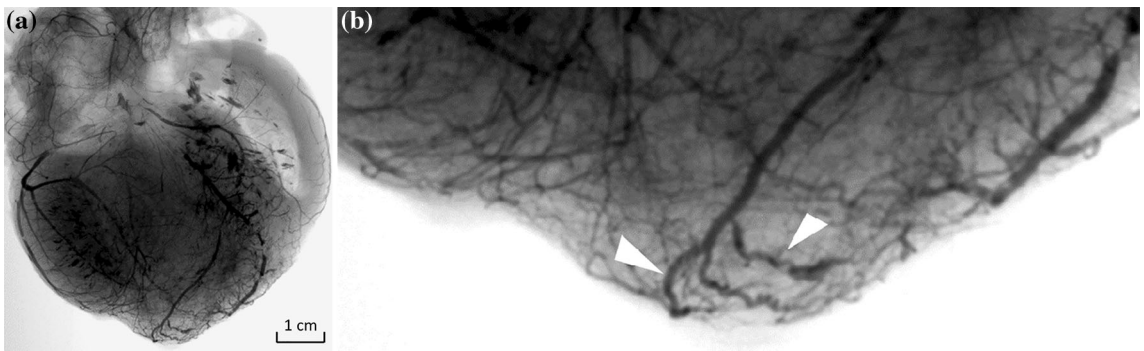

Fig. 8 An excised heart of a canine treated with c-kit-positive cardiac stem cells (CSC group). **a** The excised canine heart of the CSCs group was exposed by the cerium anode X-ray system. **b** This is a magnified image of (**a**). Numerous microvessels were visualized at the ischemic area in all canines in the CSC group. These newly formed vessels are characterized by irregularities as indicated by *white arrows*

material because it has a K-edge at 37.4 keV. We had to fill the coronary microvessels, and needed a contrast material which remains in the vascular bed. Concentrated barium with higher viscosity can fill microvessels and remain in the vessels. Barium is never used for intravenous injections in clinical settings. However, the heart was excluded immediately after the barium contrast materials had been injected, and, therefore, the animal models were not physiologically affected by the barium contrast materials. Barium contrast materials were concentrated before the injection in the vessels, and, consequently, the concentrated barium was able to remain in the vessels for a period.

Evaluation of coronary microvessels by the cerium anode X-ray system

According to the microangiography of excised hearts from normal canines (Figs. 2, 3, 4, 5), the cerium anode X-ray system allowed visualization of coronary microvessels down to third-order branches of IMCA. The difference in the ability to detect IMCAs between the two X-ray systems became more apparent if we added a 20-cm-thick acrylic plate in front of the detector to simulate X-ray absorption by the human body (Figs. 4, 5; Table 1).

Concerning the spatial resolution of the cerium anode X-ray system, noteworthy observations are shown in Table 1. A drastic reduction of the mean vessel diameter of 72.7% (from 319.5 to 86.7 μm) was noted at the branching from the EPCA to first-order branches of IMCA. On the other hand, a smaller reduction of the mean diameter of 27.7% (from 78.6 to 55.2 μm) at the branching junction of first- and second-order branches of IMCA, and 30.9% (from 75.0 to 52.4 μm) at the branching junction of second- and third-order branches of IMCA. Both the reduction rates were comparable with those reported by Tanaka et al. [21]. However, the number of the detected branches reduced to 44 of first-order, 28 of second-order, and 14 of third-order branches at branching. These observations suggest that the cerium anode X-ray system could visualize and measure down to second- or third-order branches of IMCA, but 50 μm of the spatial resolution of the cerium anode X-ray system is too poor to accurately measure the diameters of all the second- or third-order branches of IMCA. More precise detectors and more photon flux might

improve the accuracy of diameter measurements of smaller vessels of second- or third-order branches of IMCA.

Assessment of the effects after the regenerative therapy by the cerium anode X-ray system

The experimental study using the c-kit-positive cells revealed that they replaced the damaged tissue and improved the left ventricle function [9]. Hosoda et al. reported newly formed myocytes and the regeneration of myocardium after the injection of c-kit-positive cardiac progenitor cells.

According to the report on the SCIPIO trial, the effectiveness of the CSCs injection was evaluated by the indices of the left ventricular ejection fraction, the infarct size, and the left ventricle mass, measured by the 1.5 T MRI [11]. However, so far, the microvessels which are thought of as newly formed vessels are not evaluated by imaging methods. Additionally, PET CT has also been considered for imaging labeled circulating cells, but it has relatively poor spatial resolution [22].

The cerium anode X-ray system allowed the visualization of small regenerated vessels induced by c-kit-positive CSCs injected after myocardial ischemia (Fig. 8) which were not present in the control ischemic animals not treated with CSCs (Fig. 7). Furthermore, the cerium anode X-ray system has the ability to visualize microvesssels, exposing wide portions of the heart. Therefore, the form in which the microvessels were running could also be evaluated. Thus, the cerium anode X-ray system may be useful for elucidating the regeneration of small vessels.

In the present study, cardiac wall motion was not improved in the CSC group 1 month after the operation. This result raised two possibilities. One is that the regenerated vessels were not sufficient to recover the left ventricular movement, and the other is that the vessels developed after myocardial necrosis. This remains unclear, since detailed examination for cardiac function was not conducted in this study.

The clinical application of the cerium anode X-ray system

In the future, ischemic heart disease will be treated by reconstruction concomitant with regenerative therapy. However, for now, the evaluative method is insufficient compared to the progress of regenerative therapy [4]. The new system which can evaluate coronary microvessels will be needed more, especially in clinical settings. The cerium anode X-ray system is thought to be useful particularly in evaluating the coronary microvessels after regenerative therapy. There are some possibilities for the cerium anode X-ray system used in clinical settings. It will lead to earlier judgement of the treatment effectiveness, reducing patient burden both physically and mentally, excluding unnecessary treatment, and reducing the medical cost. Iodine contrast materials, which are widely used in clinical settings, could also be used for the cerium anode X-ray system. The system does not require a large facility. Additionally, it is easily operated in a few minutes.

For applying the cerium anode X-ray system in clinical settings, some points should be overcome. First, the system should have a finer detector to quantitate the diameter of the small vessels, and, in turn, X-ray intensity should be increased. Second, the number of the studied animals are too small as a preclinical study prior to clinical application. Third, involvement of the industry is necessary toward future clinical application.

Limitation

There are a few limitations in the present study. We did not perform real-time imaging but only did snap shots of the excised hearts. We recently performed real-time imaging of cerebral angiography and visualized perforating branches from the middle cerebral artery and cortical branches. We need further studies before clinical application of the cerium anode X-ray system.

Conclusions

In conclusion, the present study demonstrated the advantages of the cerium anode X-ray system to visualize small intramural coronary arteries, and possibly it can visualize angiogenic vessels induced by c-kit positive cells therapy.

Acknowledgements The study was supported by Grants-in-Aid for Scientific Research B (20390336, 2007–2010), Grant-in-Aid for Young Scientists B (25861233, 2013–2014), and Grants-in-Aid from The Cardiovascular Research Fund, Tokyo, Japan (H24-06-01, 2013–2014). Additionally, it was partly supported by a research grant from Health and Labour Sciences Research Grant (200624005A, 2004–2006) and The Research Funding for Longevity Sciences from National Center for Geriatrics and Gerontology (NCGG), Japan (22-5, 2010–2012). We would like to acknowledge Masaki Inoue, Emiko Hayashi (Tokai University Institute of Innovative Science and Technology, Kanagawa, Japan), Sachie Tanaka, Yoko Takahari, Yoshiko Shinozaki, Katsuko Naito (Support Center for Medical Research and Education, Tokai University School of Medicine, Kanagawa, Japan), Fujio Ando and Rie Hasegawa (Tokai University Imaging Center, Kanagawa, Japan), who contributed to the experiments.

Author contributions Design of study; CT, TH, HM. Experiment; CT, TH, YI, YS, KT, TS, TS. NF, HM. Data collecting and analyzing; CT, KT, HM, Drafting the article; CT, TH, HM.

Compliance with ethical standards

Funding This study was funded by Grants-in-Aid for Scientific Research B (20390336, 2007–2010), Grant-in-Aid for Young Scientists B (25861233, 2013–2014), and Grants-in-Aid from The Cardiovascular Research Fund, Tokyo, Japan (H24-06-01, 2013–2014). Additionally, it was partly supported by a research grant from Health and Labour Sciences Research Grant (200624005A, 2004–2006) and The Research Funding for Longevity Sciences from National Center for Geriatrics and Gerontology (NCGG), Japan (22-5, 2010–2012).

Conflict of interest The authors declare that they have no conflict interest other than the funding mentioned above.

Research involving animals All procedures performed in studies involving animals were in accordance with the ethical standards of the institution or practice at which the studies were conducted.

Informed consent This article does not contain any studies with human participants.

References

1. Borisenko O, Wylie G, Payne J, Bjessmo S, Smith J, Firmin R, Yonan N (2014) The cost impact of short-term ventricular assist devices and extracorporeal life support systems therapies on the National Health Service in the UK. Interact Cardiovasc Thorac Surg 19:41–48
2. Khazanie P, Hammill BG, Patel CB, Eapen ZJ, Peterson ED, Rogers JG, Milano CA, Curtis LH, Hernandez AF (2014) Trends in the use and outcomes of ventricular assist devices among medicare beneficiaries, 2006 through 2011. J Am Coll Cardiol 63:1395–1404
3. Alba AC, Alba LF, Delgado DH, Rao V, Ross HJ, Goeree R (2013) Cost-effectiveness of ventricular assist device therapy as a bridge to transplantation compared with nonbridged cardiac recipients. Circulation 127:2424–2435
4. John VF, Roger JH (2004) In vivo tracking of stem cells for clinical trials in cardiovascular disease. Circulation 110:3378–3383
5. Rosalinda M, Linda WVL, Sean MD, Felix BE, Derek JH, Sandrine L, Jonathan L, Cinzia P, Rainer S, Kirsti Y, Ulf L, Christine LM, Stefan J, James W, Thomas E, Péter F, Joost PGS (2016) Position paper of the european society of cardiology working group cellular biology of the heart: cell-based therapies for myocardial repair and regeneration in ischemic heart disease and heart failure. Eur Heart J. doi:10.1093/eurheartj/ehw113
6. Choi SH, Jung SY, Kwon SM, Baek SH (2012) Perspectives on stem cell therapy for cardiac regeneration. Adv Chall Circ J 76:1307–1312
7. Hosoda T (2012) C-kit-positive cardiac stem cells and myocardial regeneration. Am J Cardiovasc Dis 2:58–67
8. Burridge PW, Keller G, Gold JD, Wu JC (2012) Production of de novo cardiomyocytes: human pluripotent stem cell differentiation and direct reprogramming. Cell Stem Cell 10:16–28
9. Bearzi C, Rota M, Hosoda T, Tillmanns J, Nascimbene A, De Angelis A, Yasuzawa-Amano S, Trofimova I, Siggins RW, Lecapitaine N, Cascapera S, Beltrami AP, D'Alessandro DA, Zias E, Quaini F, Urbanek K, Michler RE, Bolli R, Kajstura J, Leri A, Anversa P (2007) Human cardiac stem cells. Proc Natl Acad Sci USA 104:14068–14073
10. Bearzi C, Leri A, Lo Monaco F, Rota M, Gonzalez A, Hosoda T, Pepe M, Qanud K, Ojaimi C, Bardelli S, D'Amario D, D'Alessandro DA, Michler RE, Dimmeler S, Zeiher AM, Urbanek K, Hintze TH, Kajstura J, Anversa P (2009) Identification of a coronary vascular progenitor cell in the human heart. Proc Natl Acad Sci USA 106:15885–15890
11. Bolli R, Chugh AR, D'Amario D, Loughran JH, Stoddard MF, Ikram S, Beache GM, Wagner SG, Leri A, Hosoda T, Sanada F, Elmore JB, Goichberg P, Cappetta D, Solankhi NK, Fahsah I, Rokosh DG, Slaughter MS, Kajstura J, Anversa P (2011) Cardiac stem cells in patients with ischaemic cardiomyopathy (scipio): initial results of a randomised phase 1 trial. Lancet 378:1847–1857
12. Chugh AR, Beache GM, Loughran JH, Mewton N, Elmore JB, Kajstura J, Pappas P, Tatooles A, Stoddard MF, Lima JA, Slaughter MS, Anversa P, Bolli R (2012) Administration of cardiac stem cells in patients with ischemic cardiomyopathy: the scipio trial: surgical aspects and interim analysis of myocardial function and viability by magnetic resonance. Circulation 126:S54–S64
13. Mori H, Hyodo K, Tanaka E, Uddin-Mohammed M, Yamakawa A, Shinozaki Y, Nakazawa H, Tanaka Y, Sekka T, Iwata Y, Handa S, Umetani K, Ueki H, Yokoyama T, Tanioka K, Kubota M, Hosaka H, Ishikawa N, Ando M (1996) Small-vessel radiography in situ with monochromatic synchrotron radiation. Radiology 201:173–177
14. Mori H, Hyodo K, Tobita K, Chujo M, Shinozaki Y, Sugishita Y, Ando M (1994) Visualization of penetrating transmural arteries in situ by monochromatic synchrotron radiation. Circulation 89:863–871
15. Abudurexiti A, Kameda M, Sato E, Abderyim P, Enomoto T, Watanabe M, Hitomi K, Tanaka E, Mori H, Kawai T, Takahashi K, Sato S, Ogawa A, Onagawa J (2010) Demonstration of iodine k-edge imaging by use of an energy-discrimination x-ray computed tomography system with a cadmium telluride detector. Radiol Phys Technol 3:127–135
16. Matsukiyo H, Watanabe M, Sato E, Osawa A, Enomoto T, Nagao J, Abderyim P, Aizawa K, Tanaka E, Mori H, Kawai T, Ehara S, Sato S, Ogawa A, Onagawa J (2009) X-ray fluorescence camera for imaging of iodine media in vivo. Radiol Phys Technol 2:46–53
17. Nakajima Y, Akizuki N, Kimura Y, Kohguchi H, Tanaka A, Chujo M, Hattan N, Shinozaki Y, Iida A, Handa S, Nakazawa H, Mori H (1999) Intramyocardial vascular volume distribution studied by synchrotron radiation-excited x-ray fluorescence. Am J Physiol 277:H2353–H2362
18. Mori H, Haruyama S, Shinozaki Y, Okino H, Iida A, Takanashi R, Sakuma I, Husseini WK, Payne BD, Hoffman JI (1992) New nonradioactive microspheres and more sensitive x-ray fluorescence to measure regional blood flow. Am J Physiol 263:H1946–H1957
19. Myojin K, Taguchi A, Umetani K, Fukushima K, Nishiura N, Matsuyama T, Kimura H, Stern DM, Imai Y, Mori H (2007) Visualization of intracerebral arteries by synchrotron radiation microangiography. Am J Neuroradiol 28:953–957
20. Sato E, Tanaka E, Mori H, Kawai T, Ichimaru T, Sato S, Takayama K, Ido H (2004) Demonstration of enhanced k-edge angiography using a cerium target x-ray generator. Med Phys 31:3017–3021
21. Tanaka A, Mori H, Tanaka E, Mohammed MU, Tanaka Y, Sekka T, Ito K, Shinozaki Y, Hyodo K, Ando M, Umetani K, Tanioka K, Kubota M, Abe S, Handa S, Nakazawa H (1999) Branching patterns of intramural coronary vessels determined by microangiography using synchrotronradiation. Am J Physiol 276(6 Pt 2):H2262–H2267
22. Ian YC, Joseph CW (2011) Cardiovascular molecular imaging focus on clinical translation. Circulation 123:425–443